

First results from the equatorial geomagnetic station at Entoto Observatory and Research Center

Amoré Nel^{1,2}, Nigussie Giday³, Marcos Da Silva⁴, Daniel Chekole³, Jürgen Matzka⁴, Ziyaad Isaacs¹, Oliver Bronkala⁴, and Lamessa Mogasa³

¹South African National Space Agency (SANSA), South Africa.

²Center for Space Research, North-West University, Potchefstroom, 2522, South Africa.

³Department of Space and Planetary Science, Space Science and Geospatial Institute (SSGI), Addis Ababa, Ethiopia.

⁴GFZ German Research Centre for Geosciences, Potsdam, Germany.

Correspondence: Amoré Nel (anel@sansa.org.za)

Abstract. This paper presents the initial results from the newly deployed Entoto Magnetometer Station near Addis Ababa, Ethiopia, a collaborative project involving the South African National Space Agency (SANSA), the Space Science and Geospatial Institute (SSGI) in Ethiopia, and the German Centre for Geosciences (GFZ). The station, equipped with a LEMI-025 fluxgate magnetometer and a GSM-90 Overhauser sensor, aims to monitor geomagnetic field variations and enhance space weather research in the African sector. This deployment is a significant step in SANSA's efforts to establish a comprehensive geomagnetic network across Africa, contributing to global space weather models. This is of particular importance, as the Entoto station is, to our knowledge, the only currently operational magnetic station near the dip equator in the African region, positioning the Entoto Observatory and Research Center at SSGI as a key contributor to regional and global geomagnetic research. Early observations show a good characterization of geomagnetic disturbances, with observed field changes aligning closely with the Dst index variations, which has important implications for space weather forecasting. The station also generates local K-index data for this region, providing valuable insights into ionospheric variability and its effects on technological systems. This paper details the station's setup, data processing methodologies, and initial scientific results, laying the foundation for future research and collaboration in this critical area of space science.

1 Introduction

The Earth's magnetic field plays a crucial role in shielding the planet from solar radiation and influencing space weather (Kamide, 2001; Kotzé et al., 2015). Generated primarily by the geodynamo in the Earth's liquid core, this field extends from the core through the planet's surface into space, where it interacts with solar wind and cosmic radiation. Other contributing sources include electrical currents in the ionosphere and magnetosphere, magnetized crustal rocks, and induced currents in the mantle and oceans. These internal and external sources collectively shape the geomagnetic field. Secular variation, the slow temporal change in the magnetic field, provides insight into the geodynamo's behavior, making long-term monitoring essential for understanding natural processes and the technological impacts of space weather (Nel et al., 2024).

23 Ground-based geomagnetic observatories are vital for monitoring these variations. High-quality data from observatories have
24 been instrumental in studying secular variation and disturbances such as geomagnetic storms (Matzka et al., 2010; Nel and
25 Kotzé, 2024). Despite their importance, the global network of observatories faces challenges, particularly in under-monitored
26 regions like Africa and the Southern Hemisphere (Giday et al., 2020; Yizengaw and Moldwin, 2009). The scarcity of observa-
27 tions in these areas underscores the need for new stations, especially near the magnetic equator, where space weather strongly
28 influences the ionosphere (Mungufeni et al., 2018; Macmillan, 2007). The establishment of the Entoto Magnetometer Station
29 in Ethiopia addresses this gap. Located near the magnetic equator, the station is part of SANSa's broader efforts to improve re-
30 gional space weather forecasting. This collaborative initiative between SANSa, Ethiopia's SSGI, and Germany's GFZ, aims to
31 generate high-quality geomagnetic data to fill critical gaps in the global network. By capturing geomagnetic variations specific
32 to the African sector, the Entoto station enhances both regional and global space weather models, contributing to improved
33 predictions of geomagnetic storms and their effects on technological systems, including communication networks and power
34 grids (Matzka et al., 2010).

35 Several research fields are essential for understanding geomagnetic phenomena, particularly near the magnetic equator. Among
36 these are studies of the equatorial ionosphere, equatorial plasma bubbles (Giday et al., 2020), geomagnetic storms, solar quiet
37 (Sq) variations, the Equatorial Electrojet (EEJ), and the counter-equatorial electrojet (Habarulema et al., 2019). The EEJ, in
38 particular, is of significant interest as it represents a concentrated eastward electric current superimposed on the global Sq
39 current system. The relationship between the global Sq current system and the EEJ remains a subject of active research and
40 ongoing debate (Yamazaki and Maute, 2016). Understanding the interactions between these currents is critical for improving
41 models of ionospheric conductivity, geomagnetic variations, and space weather impacts on equatorial regions.

42 Despite the importance of such studies, Africa faces a persistent challenge due to the lack of active magnetometer stations along
43 the magnetic equator. Currently, there are no operational magnetometer stations in the region with the necessary capabilities to
44 effectively study Sq variations and the EEJ. Existing networks, such as the MAGnetic Data Acquisition System (MAGDAS)
45 and the International Real-time Magnetic Observatory Network (INTERMAGNET), include a limited number of stations in
46 Africa, but many are either inactive or positioned at latitudes too far from the equator to capture equatorial phenomena accu-
47 rately.

48 For instance, there are two INTERMAGNET observatories in northern Africa: one in Ethiopia, one in Mbour, Senegal (Oper-
49 ated by IPGP), and one in Tamanrasset, Algeria (Operated by IPGP and CRAAG). However, both the Ethiopian and Senegalese
50 stations have ceased recording data, and the Algerian station is located too far from the magnetic equator to be useful for equa-
51 torial studies. Similarly, the MAGDAS and African Meridian B-Field Education and Research (AMBER) networks, which
52 previously had several stations along the magnetic equator, have experienced prolonged inactivity. As a result, Ethiopia cur-
53 rently lacks a functioning pair of low-latitude and equatorial stations, both of which are crucial for accurately studying EEJ
54 dynamics and Sq variations.

55

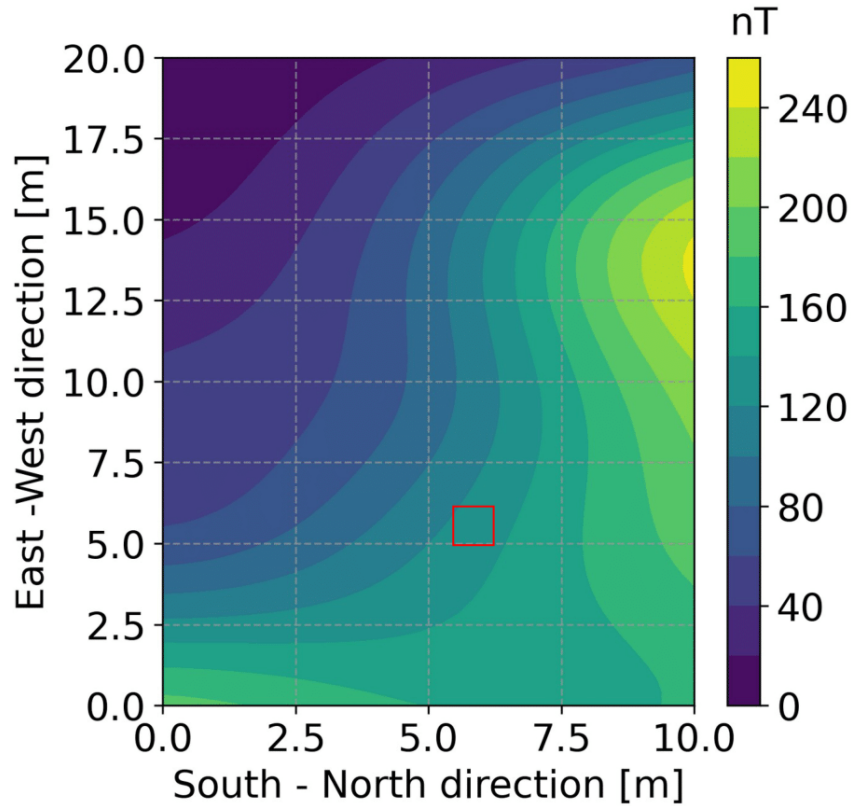


Figure 1. Magnetic gradient survey of the Entoto Observatory area ($9^{\circ}06'33.6'' N, 38^{\circ}48'24.1'' E$). The selected station location (marked) lies outside the highest-gradient region. Although peak gradients in the NW sector exceed 200 nT/m, the final site was chosen for minimal interference and is suitable for a variometer station intended for space weather monitoring and absolute observatory criteria (e.g. <1 nT/m) are not strictly required in this context.

56 The scarcity of operational equatorial magnetometer stations in Africa presents a major obstacle to advancing geomagnetic
 57 and space weather research in the region (Hamid et al., 2014a; Myint et al., 2022a; Mungufeni et al., 2018). Without high-
 58 resolution, continuous ground-based observations, researchers must rely on satellite data, which, while valuable, lacks the
 59 temporal resolution necessary for detailed EEJ and Sq variation analysis. Additionally, the absence of equatorial ground-based
 60 measurements limits the ability to validate global geomagnetic models and weakens Africa's contribution to international space
 61 weather monitoring efforts.

62 The establishment of the Entoto Magnetometer Station represents a significant step toward addressing this gap. By providing
 63 high-frequency geomagnetic measurements from a location near the magnetic equator, the station enables in-depth investiga-
 64 tions of the EEJ, Sq variations, and their interactions with global and regional space weather phenomena. The station's data will
 65 contribute to both regional forecasting and global geomagnetic modeling, enhancing our understanding of equatorial electro-



Figure 2. Magnetometer Setup: The magnetometer is housed in a protective structure designed to withstand environmental challenges, including potential flooding, and to maintain temperature stability. Data is logged continuously and transferred to the respective institutes for analysis and storage.

dynamics and their impact on communication, navigation, and power systems. This will improve the monitoring and prediction of space weather phenomena in Africa, especially in regions historically underrepresented in existing networks (Uemoto et al., 2010).

The local K-index, derived from ground-based measurements, is an essential tool for assessing local disturbance monitoring and prediction. Numerous space weather prediction centers have started measuring their local K-index using local magnetometer station data, in order to do regional forecasting: Unlike the planetary Kp-index, which averages data from multiple observatories worldwide, the local K-index provides region-specific insights into geomagnetic activity. For stations located near the magnetic equator, such as Entoto, the K-index must account for the unique influence of the equatorial electrojet, which can distort the magnetic field measurements used to compute the index. Recent studies, such as those conducted at the Phuket station in Thailand, have demonstrated the importance of selecting appropriate calibration values for generating accurate local K-indices in equatorial regions (Hamid et al., 2014b; Myint et al., 2022b). One of the key challenges in computing the local K-index near the equator is determining the lower limit (L_9 , which is defined as the lower $K = 9$ threshold value) for the K-index scale, which varies with geomagnetic latitude. Equatorial stations require higher L_9 values due to the strong influence of the EEJ, which can otherwise lead to an overestimation of geomagnetic disturbances. At the Entoto station, the analysis of the local K-index will provide critical insights into the day-to-day variability of the EEJ and its impact on geomagnetic activity.

81 By generating accurate local K-indices, the station will enhance regional space weather prediction capabilities, particularly in
82 terms of forecasting geomagnetic storms that could disrupt communication systems and power grids. Additionally, the data
83 collected at Entoto will contribute to a broader understanding of how geomagnetic disturbances evolve in the African sector,
84 filling a critical gap in the global geomagnetic observation network (Menvielle et al., 1995).

85 The establishment of the Entoto magnetometer station marks a significant milestone in the advancement of geomagnetic re-
86 search in Africa (Hamid et al., 2014a; Myint et al., 2022a; Mungufeni et al., 2018). By providing high-quality data on the local
87 K-index and geomagnetic field variations, the station will play a pivotal role in improving space weather prediction capabilities
88 both regionally and globally. The collaboration between SANSa, the SSGI, and the GFZ highlights the importance of regional
89 efforts in addressing the global challenges posed by space weather.

90 2 Site Selection and Instrumentation

91 A geomagnetic station is where the geomagnetic field vector is recorded continuously over a long period of time (Matzka et al.,
92 2010). Ideally, the site should be free from any static disturbances caused by local anomalies, as well as far away from human
93 traffic that could cause temporal disturbances.

94 The Entoto Observatory, established in 2014 as one of the facilities of the then Ethiopian Space Science and Technology
95 Institute (now the Space Science and Geospatial Institute (SSGI)) represents a key step in advancing the nation's space science
96 research. Funded by the Ethiopian government, along with support from universities, international partners, and private donors,
97 the observatory offers the necessary infrastructure for research in space science, geospatial technologies, and astronomy.

98 Located at the highest point in Addis Ababa, at an elevation of 3200 metres above sea level, it reflects SSGI's commitment
99 to research and positions Ethiopia as a leader in regional and global space science. The Entoto Observatory is situated approxi-
100 mately 15 km northeast of Addis Ababa. Its location away from local settlements and adjacent to Entoto National Park ensures
101 minimal interference from local magnetic noise.

102 A magnetic gradient survey was conducted (see Figure 1) and a deployment site was identified within the original section
103 of the Entoto Observatory in the northwestern sector ($9^{\circ}06'33.6''\text{N}$, $38^{\circ}48'24.1''\text{E}$). It is about 20 meters from the western
104 perimeter fence and 15 meters from an abandoned hut.

105 The magnetic gradient survey (Figure 1) revealed localised regions of elevated gradients, with values exceeding 10 nT/m
106 in the northwestern sector of the original Entoto site. While this surpasses the 1 nT/m threshold typically recommended for
107 absolute geomagnetic observatories (Jankowski and Sucksdorf, 1996), that criterion is specifically intended for baseline qual-
108 ity installations contributing to the global magnetic reference network. In contrast, the Entoto deployment is not intended to
109 operate as an INTERMAGNET-grade observatory, but rather as a variometer station focused on monitoring relative magnetic
110 field variations for space weather research. In this context, moderate gradients, although not ideal, are acceptable, as variometer
111 measurements are generally robust to static field anomalies.

112 The selected deployment site was carefully positioned just outside the steepest gradient zone, where *in situ* testing confirmed
113 improved magnetic cleanliness. The primary scientific objective is to capture dynamic ionospheric and magnetospheric field

114 perturbations, particularly those associated with phenomena such as the Equatorial Electrojet (EEJ), for which relative stability
 115 is more critical than absolute accuracy. Furthermore, future infrastructure plans include relocating the station to the western
 116 section of the Entoto campus, where the construction of new perimeter fencing and expanded facilities will allow for a 100 m
 117 buffer from any surrounding structures, significantly improving the site’s magnetic environment and long term suitability.

118 The protective structure for the proposed magnetometer station is based on the design of SANSA’s protective structure at our
 119 INTERMAGNET observatory in Keetmanshoop (KMH) (Korte et al., 2009). Some adjustments were made to this structure,
 120 for example, to compensate for potential flooding which could occur in Addis Ababa. The original structure was designed to
 121 be buried underground, the new structure will be above ground, with ample area underneath the floor for sudden water flow.
 122 Better venting pipes were designed for temperature stability.

123 **2.1 Temperature stability and correction**

124 Fluxgate magnetometers are thermally sensitive, and venting pipes alone do not ensure long-term stability. To quantify the
 125 thermal environment at Entoto, we analysed the co-located sensor (T1) and electronics (T2) temperatures. Daily ranges were
 126 modest, with median values of $\sim 3.5^{\circ}\text{C}$ (95th percentile 4.9°C) for T1 and $\sim 4.6^{\circ}\text{C}$ (95th percentile 7.2°C) for T2 (Table 1).
 127 This corresponds to an estimated median peak-to-peak effect of only ~ 2.6 nT on the H component. A representative average
 128 daily profile is shown in Figure 3, illustrating the moderated diurnal cycle inside the enclosure.

Table 1. Summary of daily temperature ranges inside the Entoto enclosure over the analysed period. Values are in $^{\circ}\text{C}$.

Quantity	Median	Mean	95th Percentile
T1 (Sensor) Range	3.5	3.6	4.9
T2 (Electronics) Range	4.6	4.8	7.2

129 To mitigate residual thermal effects, we derived temperature coefficients using co-located sensors and quiet-day analysis.
 130 The H component showed a coefficient of -0.733 nT $^{\circ}\text{C}^{-1}$, while HE and Z contributions were negligible. As illustrated in
 131 Figure 4, applying this coefficient to H reduces the small daily variation in ΔF (about 2 nT on a quiet day) and lowers its
 132 correlation with temperature. The effect is subtle, and in some cases the corrected values show slightly more scatter, which
 133 likely reflects additional baseline adjustments in the calibration workflow rather than the temperature correction itself.

134 Importantly, the correction does not degrade the data quality, and the overall ΔF variation remains dominated by geophysical
 135 signal rather than thermal artefacts.

136 Even after correction, ΔF offsets of $\sim 6\text{--}8$ nT remain, reflecting uncertainties in baseline estimation and sensor differences
 137 rather than thermal effects. We therefore consider the enclosure and correction procedure adequate for variometer-grade oper-
 138 ation, while acknowledging that this does not reach observatory-grade stability.

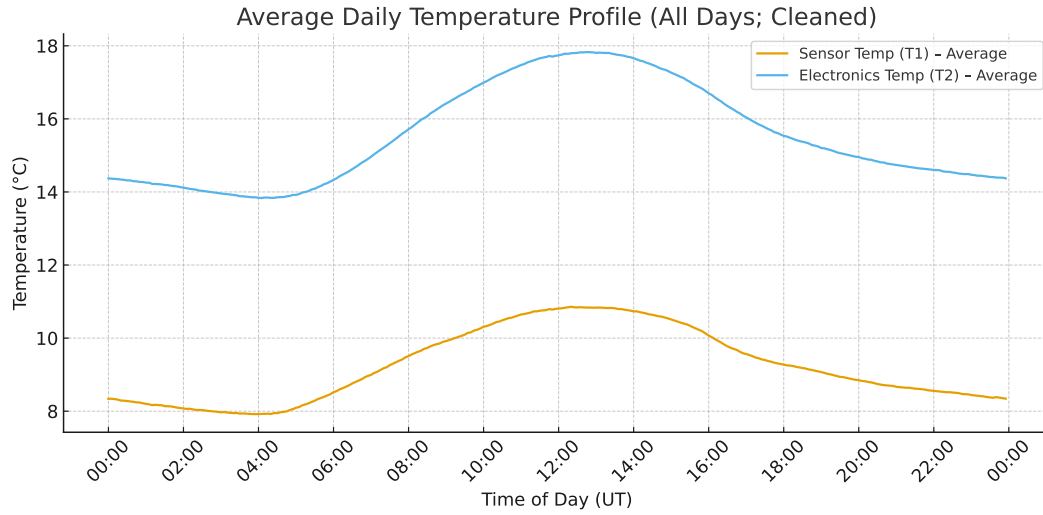


Figure 3. Average daily temperature profile inside the Entoto station enclosure, derived from all days of the last months .sec data (09-08-2025 to 09-09-2025). Sensor temperature (T1) and electronics temperature (T2) both show modest diurnal variations (median daily ranges of $\sim 3.5^{\circ}\text{C}$ and $\sim 4.6^{\circ}\text{C}$, respectively), confirming that the enclosure moderates the thermal environment.

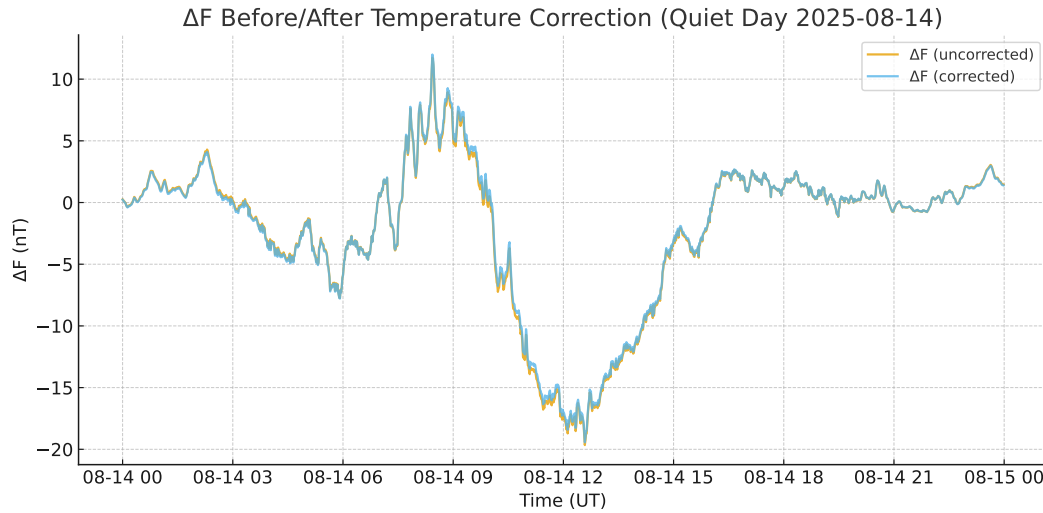


Figure 4. Comparison of ΔF uncorrected (yellow) and corrected (blue) applying the H-component temperature correction ($-0.733 \text{ nT } ^{\circ}\text{C}^{-1}$) on a representative quiet day (14 August 2025). The correction slightly reduces the small diurnal variation ($\sim 2 \text{ nT}$) and lowers correlation with temperature, consistent with the expected thermal sensitivity of fluxgate sensors.

139 2.2 Data logging and instrumentation

140 In partnership with the GFZ, a converter program for the LEMI magnetometer data recorder has been written. The station
141 currently does not include dedicated lightning protection due to the secure facility layout and non-grounded sensor cables.
142 However, lightning protection measures are under consideration for future upgrades. The LEMI-025 is connected via RS232
143 to a Linux PC and the binary data is converted to readable ASCII format. The bias signals and DAC values will be monitored
144 and checked for any anomalies.

145 The Entoto magnetometer station is equipped with a GSM-90 Overhauser sensor and a LEMI-025 fluxgate magnetometer.
146 The GSM-90 is a portable Overhauser magnetometer that measures the total magnetic field strength with high accuracy. Its
147 application varies, but for this project it's implemented for long term use and will measure the scalar signal of the local
148 geomagnetic field. The LEMI-025 is a sensitive 3-axis fluxgate magnetometer (FGM) that measures the three components of
149 the geomagnetic field (thus providing directional information) and records temporal variations at a resolution of 1 second. The
150 LEMI-025 was placed on a magnetometer pillar within the protective structure and the GSM-90 Overhauser a few metres from
151 the structure (see Figure 2) and further adjustments and testing will ensue, e.g., looking for reasonable variations, timestamps,
152 adjusting the placement of the instruments, checking for disturbances in the serial line etc. With this dual magnetometer setup
153 one can obtain both the total strength and direction of the local magnetic field, and enables a more complete understanding
154 of geomagnetic variations. Although the GSM-90 is highly accurate, it has a lower sampling rate than the LEMI-025, thus
155 combining these two sensors it provides both precision and detailed time series data. When studying space weather phenomena,
156 both the intensity and the direction of the geomagnetic field changes are crucial. Using both instruments at geomagnetic
157 observatories helps to monitor geomagnetic storms, substorms, and ionospheric phenomena effectively.

158 The sensor house comprises a reinforced structure to protect against environmental challenges. The magnetometer sensor
159 is connected to the control room via a cable, ensuring stable power supply through a power system. The magnetic field is
160 represented by its three components, North (X), East (Y), and vertical (Z), measured with respect to the local geographic
161 coordinate system, with Z being positive downward (Denardini et al., 2015). These components are digitized and logged,
162 enabling high temporal resolution analysis for space weather monitoring.

163 3 Methodology

164 The Entoto magnetometer station records variations in the geomagnetic field along the X, Y, and Z components with high tem-
165 poral resolution. These measurements enable the identification of geomagnetic activity patterns, including responses to solar
166 wind disturbances and geomagnetic storms. The collected data undergoes a series of processing steps to extract meaningful
167 geophysical signals while mitigating noise and long-term trends. The 1-minute values were computed from 1-second magne-
168 tometer data using a centered arithmetic mean, following IAGA and INTERMAGNET standards, where each value represents
169 the average of 60 samples centered on the target minute. Initial testing of the instrumentation was conducted at SANSa's
170 facilities in South Africa before deployment in Ethiopia to ensure proper calibration and data integrity.

171 Several non-geomagnetic noise sources can influence the magnetometer signal at Entoto, including temperature-induced
172 drift and anthropogenic electromagnetic interference (e.g., from nearby infrastructure or power lines). Among these, tempera-
173 ture effects are corrected through post-processing using a derived temperature coefficient for the H component. However, other
174 noise sources are more difficult to remove without risking the attenuation of the signal of interest: EEJ and Sq signals primarily
175 occupy ultra-low frequency (ULF) ranges, with dominant diurnal and semi-diurnal components below 1 mHz (Yamazaki and
176 Maute, 2016). While these frequencies are generally well-separated from anthropogenic sources such as power-line harmonics
177 (50–60 Hz) (Constable and Constable, 2023), low-frequency electronic noise can introduce artefacts in the sub-mHz band.
178 Additionally, poor shielding or digital aliasing may fold high-frequency noise into lower frequencies, complicating the reliable
179 extraction of ionospheric signals. Therefore, we adopt a conservative filtering strategy: while a high-pass filter and quiet-day
180 subtraction are applied to isolate short-term variations, no aggressive denoising is performed. This trade-off preserves the
181 geophysical integrity of the data, especially in studies focused on daily-scale variability and ionospheric current systems.

182 To isolate external geomagnetic variations, the main field, which mainly originates from the Earth’s core, is subtracted using
183 the CHAOS 8.2 model (Kloss et al., 2025). This model estimates the internal geomagnetic field at the station’s coordinates
184 during analysis and is limited to 2025.1 to avoid extrapolation. These estimated values are subtracted from the observed data
185 to obtain the corrected geomagnetic field components, removing long-term variations such as secular changes and leaving only
186 the external field perturbations. This step ensures that local geomagnetic fluctuations are not influenced by global-scale internal
187 variations.

188 To study short-term geomagnetic variations, the residual field components undergo further processing. A Butterworth high-
189 pass filter with a cutoff period of approximately 72 hours is applied to remove long-term variations. To account for solar quiet
190 variations, a quiet-day mean for each month is computed and subtracted from the dataset. Finally, a daily running mean is
191 subtracted from the data to eliminate long-period fluctuations. This process isolates daily geomagnetic variations primarily
192 influenced by ionospheric and magnetospheric currents, allowing for a more precise analysis of space weather effects.

193 To provide a broader context for local geomagnetic disturbances, the planetary Ap index is incorporated into the analysis. The
194 maximum daily Ap index values are overlaid on the corrected geomagnetic field plots, with color-coded markers indicating
195 active disturbance conditions for Ap values greater than or equal to 19 and geomagnetic storm conditions for Ap values ex-
196 ceeding 36. The integration of Ap index data allows for direct comparisons between local fluctuations and global geomagnetic
197 activity. This step is essential for correlating regional space weather phenomena with larger-scale geomagnetic disturbances
198 that could impact communication systems and navigation infrastructure.

199 3.1 Estimating the local K index

200 The K-index quantifies geomagnetic disturbances on a quasi-logarithmic scale from 0 (quiet) to 9 (strong storms). The En-
201 toto station’s local K-index is computed using the open-source MagPy software (Stolle et al., 2018) following the Finnish
202 Meteorological Institute (FMI) method, which is widely used in geomagnetic observatories. The International Association of
203 Geomagnetism and Aeronomy (IAGA) has standardized four computer-based K-index algorithms that can be applied glob-

ally. These algorithms use different solar regular (SR) curve estimation techniques. Among them, the FMI method proposed by Sucksdorff et al. (1991) is considered the most reliable compared to manual hand-scaling techniques. The FMI method is widely used for K-index generation at various observatories and serves as a baseline method for evaluating newer approaches, such as the nowcast K-index used in space weather forecasting. The FMI method employs a linear elimination approach, using geomagnetic field data from three consecutive days to estimate the SR curve for a given day.

The calculation of the local k-index using the FMI method is dependent on a station specific constant, called L_9 . This value represents the threshold geomagnetic range (in nanoTesla) that corresponds to the highest level of activity ($K = 9$) at that station. L_9 is not a dynamic variable, but a fixed value that is determined empirically using long-term historical data, typically over several years or a full solar cycle. It reflects the station's geomagnetic latitude and local environmental conditions, such as the proximity to the local EEJ. It is usually analyzed using the statistical distribution of magnetic ranges to align with global K-index conventions.

While software like MagPy can compute K-indices in realtime, it requires a pre-defined L_9 value to map the observed 3-hour range maxima to the appropriate K-level. For the Entoto station outside Addis Ababa, it is possible to use the historical L_9 value from the now decommissioned INTERMAGNET station AAE, provided that the geomagnetic environment and signal processing are comparable.

Derivation of the K-index at the Entoto station begins by importing high-resolution time series raw data at minute intervals. A baseline correction is applied and filtering to remove non-geomagnetic noise. The geomagnetic time series is then segmented into 3-hour windows, and for each interval, the maximum and minimum values of the horizontal field components are determined to compute the fluctuation range. The thresholds account for the influence of the equatorial electrojet, which can introduce distortions to standard K-index computations. Based on the fluctuation range, MagPy assigns a K-index value between 0 and 9 to each 3-hour period. This approach ensures that the K-index calculated by MagPy is both precise and station-specific, capturing local geomagnetic disturbances that may affect technological systems or contribute to space weather research.

The next few subsections outline the procedures to isolate the equatorial electrojet (EEJ) and magnetospheric contributions from low-latitude ground-based geomagnetic observations. The approach is based on removing internal and large-scale external field components from the horizontal magnetic field using the CHAOS 8.2 model, and separating diurnal (ionospheric) and nocturnal (magnetospheric) variations.

3.2 Data Preparation

Geomagnetic data with one-minute resolution from the Entoto station was used to determine the horizontal magnetic field strength. The observed horizontal magnetic field strength, H_{obs} , was computed from the orthogonal magnetic field components X and Y as:

$$H_{\text{obs}} = \sqrt{X^2 + Y^2}. \quad (1)$$

236 3.3 Internal Field Removal

237 To account for the Earth’s internal field, we used the CHAOS geomagnetic field model (Finlay et al., 2020) to estimate the
238 internal horizontal field, H_{int} , at the station’s geographic location and for each observation time. The residual horizontal field
239 was obtained by subtracting the internal field:

$$240 H_{\text{res}} = H_{\text{obs}} - H_{\text{int}}. \quad (2)$$

241 This residual field contains contributions from both ionospheric and magnetospheric sources.

242 3.4 Equatorial Electrojet Signal Extraction

243 To isolate the ionospheric EEJ signal, we selected the H_{res} values corresponding to local daytime hours, typically from 09:00
244 to 15:00 LT, when EEJ activity is strongest (Onwumechili, 1997a; Rangarajan et al., 2002). This subset of the residual field
245 represents the unrefined EEJ signal.

246 3.5 Magnetospheric Contribution Isolation

247 The nighttime portion of the residual field, spanning 18:00 to 06:00 LT, is assumed to be dominated by magnetospheric
248 contributions due to the absence of significant ionospheric currents. This signal was extracted and analyzed alongside the
249 global Dst index (Sugiura, 1964) to assess their correlation, which will be discussed in more detail in the Results section.

250 To assess the capability of the Entoto station to detect space weather effects, we generated a time series comparing the local
251 magnetospheric signal, extracted from nighttime residuals of the horizontal magnetic field, with the global Dst index. Then
252 we selected geomagnetically quiet periods ($\text{Dst} > -20$) and disturbed periods ($\text{Dst} < -50$) in order to show superposed epoch
253 plots of the EEJ signal, showing its diurnal variation averaged over each period. The first method will illustrate the station’s
254 sensitivity to global magnetospheric conditions, while the second will show how ionospheric currents (particularly the EEJ)
255 behave during quiet and disturbed times. To support this visual analysis, we will also perform two quantitative comparisons:
256 a Pearson correlation between the magnetospheric signal as measured at the station and Dst to measure the linear association,
257 and a comparison of the mean daily maximum EEJ amplitude during quiet and storm conditions. These metrics provide a
258 simple statistical measure of the station’s physical response to varying levels of geomagnetic activity.

259 4 Results and Discussion

260 Figures 3 and 4 illustrate the thermal environment and its correction at Entoto. Figure 3 shows that both the sensor (T1) and elec-
261 tronics (T2) temperatures exhibit only modest diurnal variations, while Figure 4 demonstrates that applying the H-component
262 temperature coefficient ($-0.733 \text{ nT } ^\circ\text{C}^{-1}$) slightly reduces the small daily variation in ΔF and lowers its correlation with tem-
263 perature. These results confirm that the enclosure provides adequate thermal moderation for variometer-grade operation, with
264 post-processing correction acting as an additional safeguard.

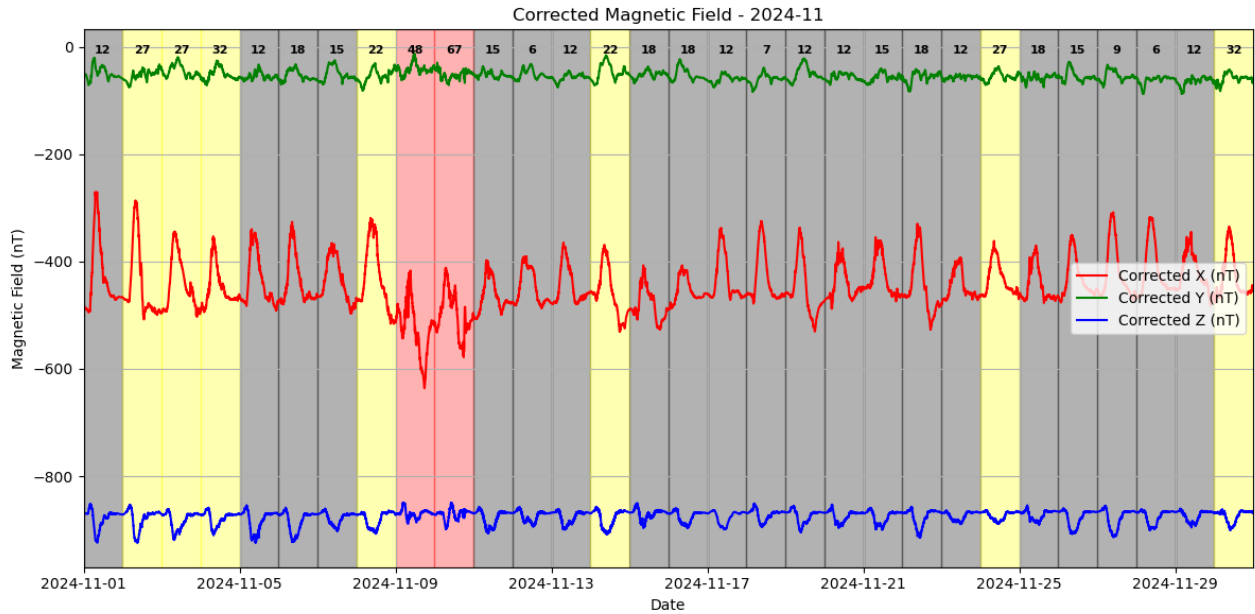


Figure 5. Variations in the local geomagnetic field along the X (red line), Y (green line), and Z (blue line) components during November 2024. At the top of the graph the daily maximum Ap value is shown. The greyed out days refer to quiet times, yellow days are unsettled, and red is disturbed days.

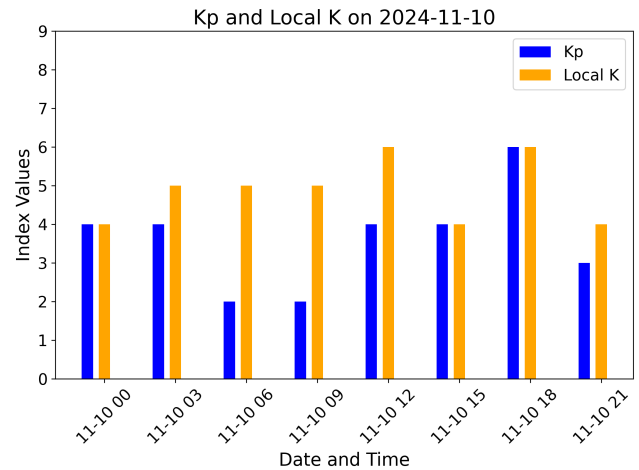
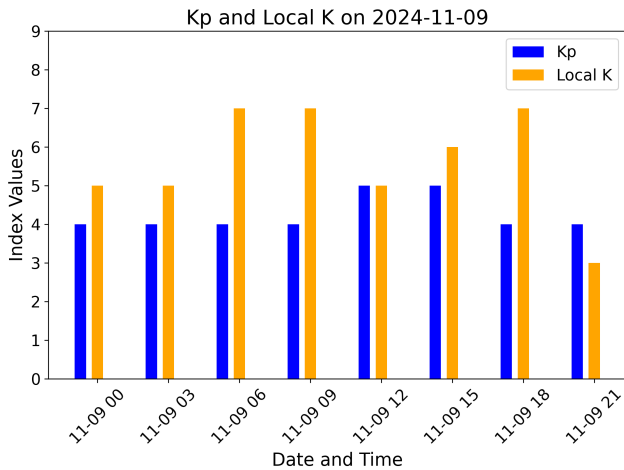


Figure 6. Kp and local K indices derived from the Entoto station. Both figures show indices as measured during disturbed storm times, as seen in Figure 5.

265 The processed diurnal variations were visualized by plotting the residual components $\Delta X, \Delta Y, \Delta Z$ against local time to
266 observe the daily geomagnetic patterns. Plots were generated for each complete month since deployment until January 2025
267 as shown in Figures 5, 7, and 9. Additionally, solar activity indices, including the Ap index, were compared with the diurnal
268 variations to evaluate the influence of solar activity on the geomagnetic field. Based on the Ap-index values, the above analyses
269 show that the geomagnetic field variations were consistent with the planetary geomagnetic activity levels. During the night, the
270 fields were generally stable for quiet days. When the geomagnetic activity was high, irregular variations were detected during
271 both daytime and nighttime.

272 The comparison between the global planetary Kp index and the locally derived K index at the Entoto station consistently
273 shows that the local K values are approximately one to two levels higher, even during geomagnetically quiet periods, shown
274 for selected times in Figures 6 and 8. This discrepancy can largely be attributed to the station's location near the magnetic
275 equator, where it is strongly influenced by the Equatorial Electrojet (EEJ). The EEJ introduces pronounced diurnal variations
276 in the horizontal component of the geomagnetic field, which are not captured in the mid-latitude stations contributing to the Kp
277 index (Forbes and Lindzen, 1981; Onwumechili, 1997b). Consequently, the Entoto station records elevated field disturbances
278 relative to global averages.

279 In the present study, a historical K9 threshold value of 242 nT, derived from the former AAE INTERMAGNET observatory
280 in Addis Ababa (latitude 9.035° N, longitude 38.77° E), was used to calculate the local K index. However, the significance
281 of this threshold is limited by the fact that the station was located at a geomagnetic latitude of less than 10°, where the EEJ
282 strongly modulates magnetic variability and distorts comparisons with mid-latitude standards. As such, this K9 value may not
283 adequately characterize the magnetospheric and ionospheric influences at low-latitude sites like Entoto. As part of future work,
284 a dedicated and empirically determined L_9 value will be established for Entoto once a longer time series of high-quality data
285 becomes available (Menvielle et al., 1995; Korte et al., 2018).

286 Figures 10, 11, and 12 show the measured magnetospheric signal of the station versus the global Dst index, the mean
287 EEJ signal during quiet ($Dst > -20$), and disturbed ($Dst < -50$) times respectively. These Figures illustrate the ability of the
288 Entoto station to capture both magnetospheric and ionospheric responses to space weather conditions. Figure 10 demonstrates
289 a moderate to strong Pearson correlation of 0.62 between the station's derived magnetospheric signal and the global Dst
290 index, indicating that the station reliably reflects variations in magnetospheric current systems. Figures 11 and 12 compare
291 the equatorial electrojet (EEJ) signal during geomagnetically quiet and disturbed periods. The mean daily maximum EEJ
292 amplitude was significantly larger during storm days (-317.9 nT) than during quiet days (-257.2 nT), suggesting that the
293 station effectively captures enhancements in the EEJ associated with storm-time ionospheric dynamics. These preliminary
294 results confirm the station's sensitivity to both global geomagnetic disturbances and regional ionospheric variability.

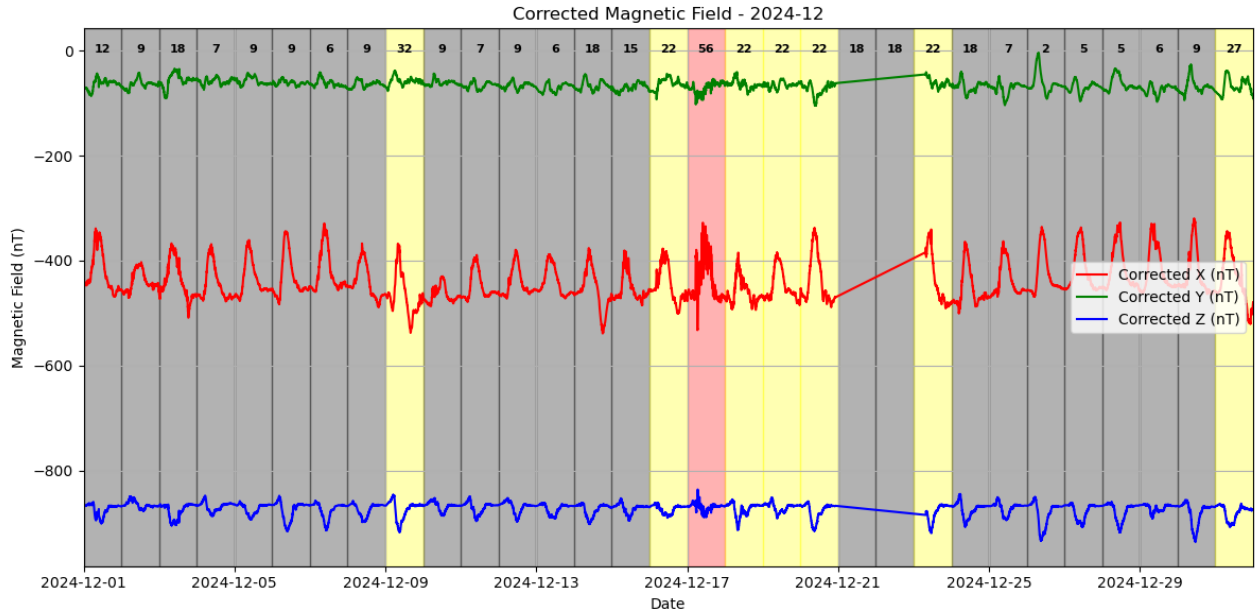


Figure 7. Variations in the local geomagnetic field along the X (red line), Y (green line), and Z (blue line) components during December 2024. As described in Figure 5

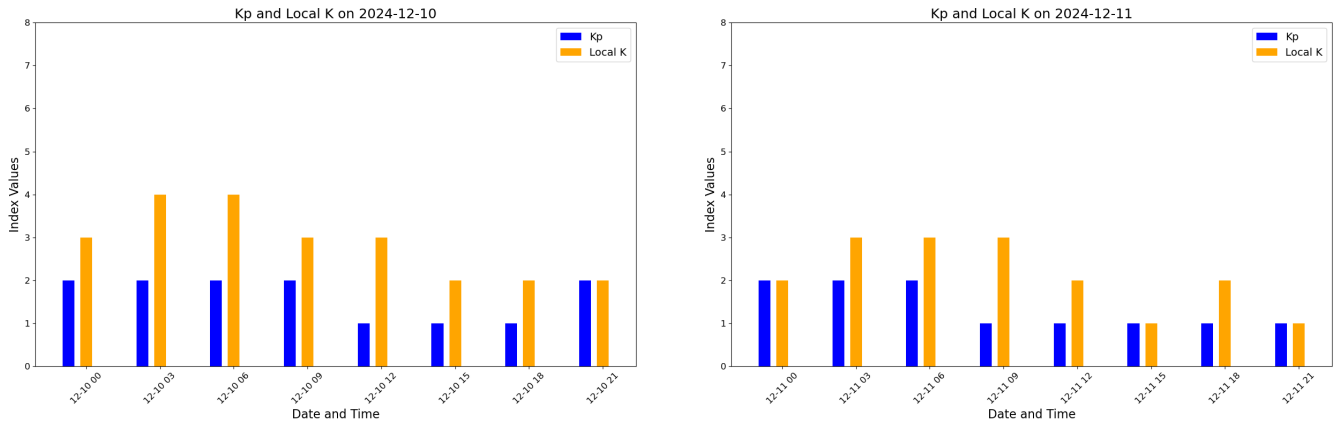


Figure 8. Kp and local K indices derived from the Entoto station. Here Figures show indices during quiet times, as seen in Figure 7.

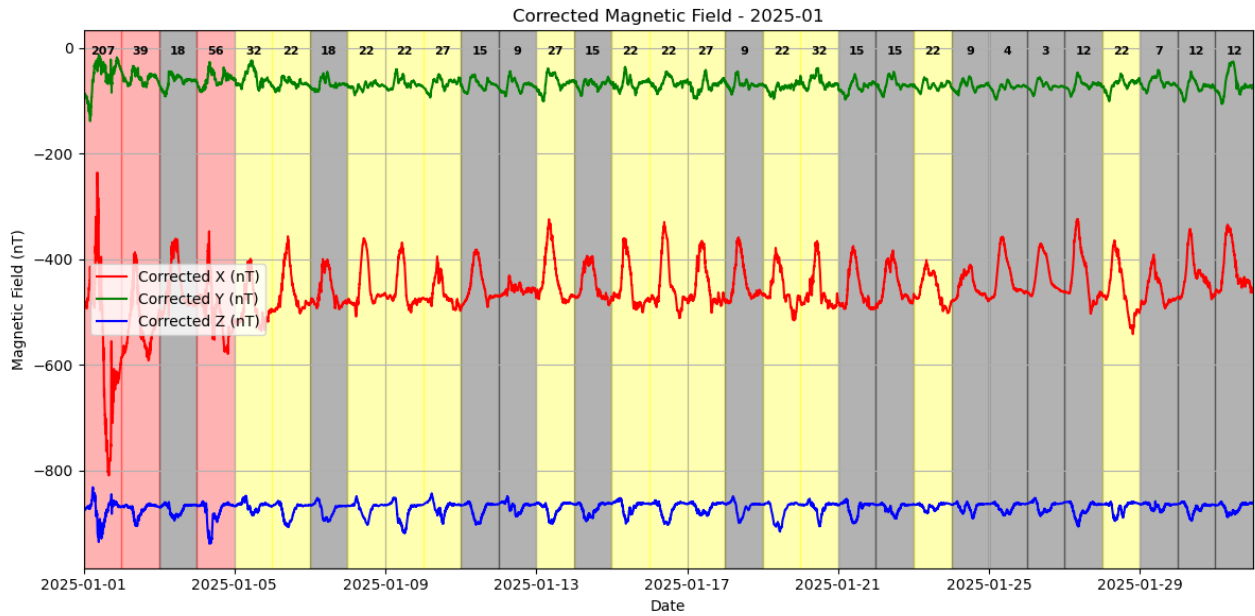


Figure 9. Variations in the local geomagnetic field along the X (red line), Y (green line), and Z (blue line) components during January 2025. As described in Figure 5

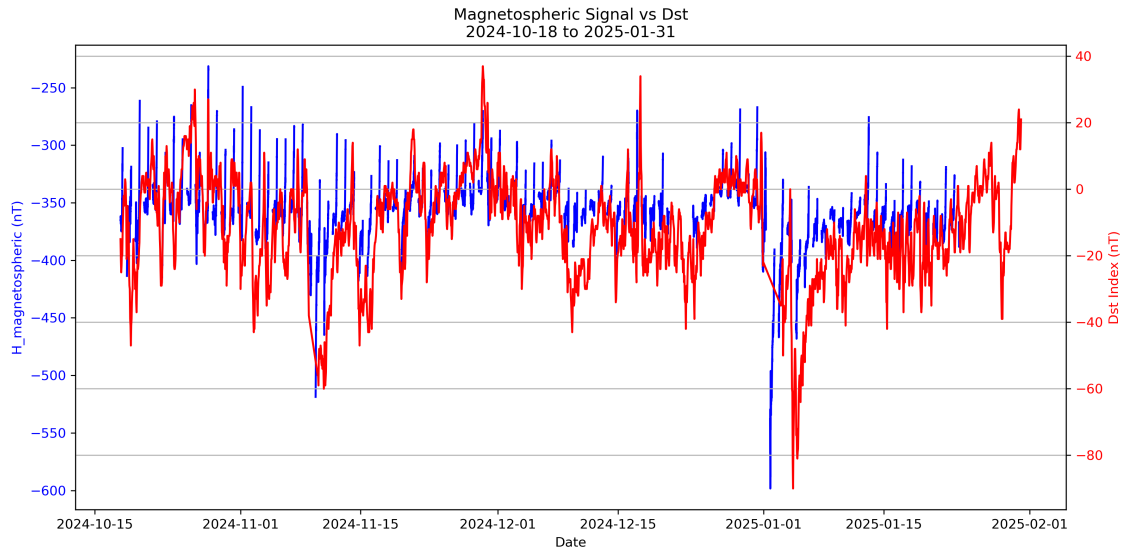


Figure 10. The measured magnetospheric signal of the station versus the global Dst index for date range 2024-10-18 to 2025-01-31

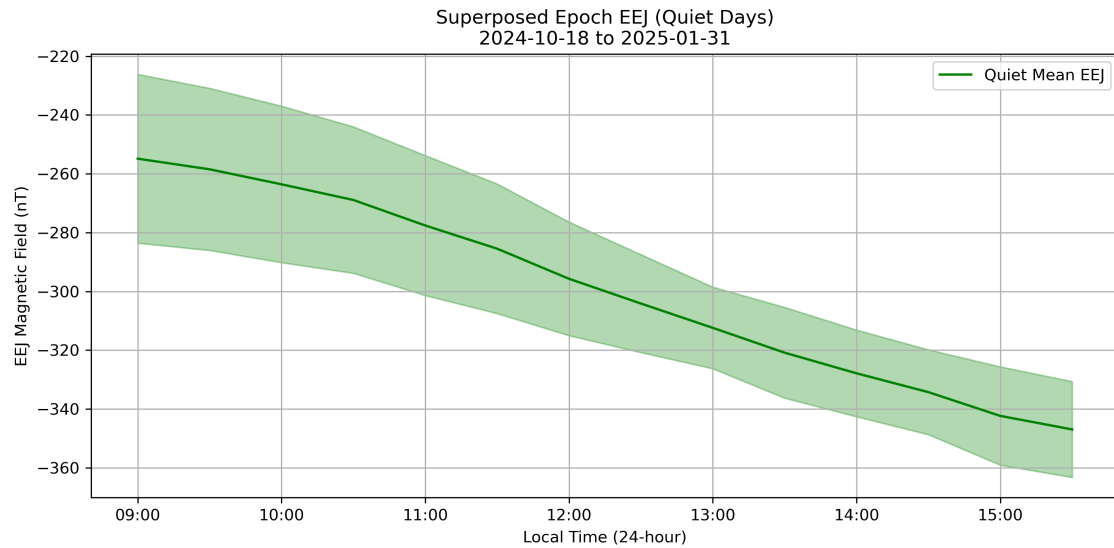


Figure 11. Mean EEJ amplitude for selected quiet geomagnetic days for the selected date range, based on the daily mean of 1-minute EEJ values. These values provide a baseline for comparison with disturbed-time EEJ enhancements.

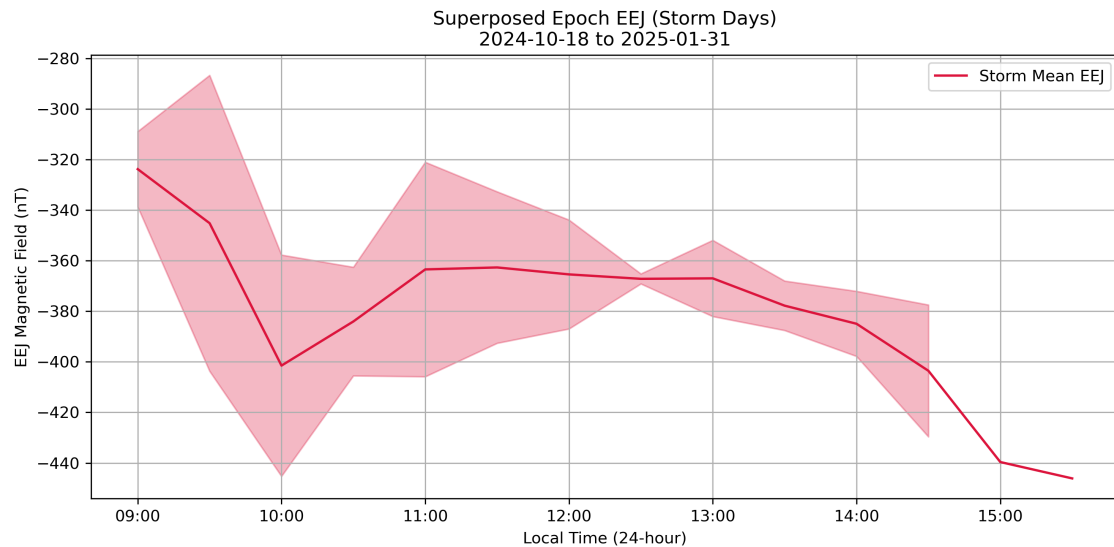


Figure 12. Mean EEJ amplitude for selected geomagnetic storm days for the selected date range, computed as the daily mean of 1-minute EEJ values from the Entoto variometer data. This captures the net enhancement of the equatorial electrojet during disturbed conditions.

295 5 Conclusion

296 Variations in the local geomagnetic field along the X, Y, and Z components were plotted alongside the maximum daily Ap
297 values. This was used to identify recurring patterns and assessing the impact of space weather over extended periods. This
298 preliminary data from the Entoto Magnetometer Station shows clear variations in the geomagnetic field, particularly during
299 periods of increased solar activity.

300 The local K-index for the Entoto station was estimated using the MagPy software and compared against the planetary K-
301 index. These results are consistent with previous studies (Kotzé et al., 2015), which have demonstrated the value of the local
302 K-index in assessing geomagnetic activity, particularly in regions with distinctive geomagnetic features. In the case of Entoto,
303 situated near the magnetic equator, the influence of the equatorial electrojet (EEJ) plays a significant role. As expected, the
304 local K-index was typically higher than the planetary K-index, both during quiet and disturbed periods. This discrepancy
305 underscores the importance of generating a station-specific L9 (K9 lower limit) value once sufficient data has been collected.
306 While this would improve the precision of the local K-index, determining an appropriate L9 value in equatorial regions is
307 inherently challenging due to the dynamic and variable nature of the EEJ.

308 While the Entoto site offers relative magnetic quiet in terms of anthropogenic noise, the gradient survey revealed localized
309 crustal anomalies with values exceeding 10 nT/m in some areas. These elevated gradients can give rise to small-scale induction
310 effects, especially during geomagnetic storms, due to variations in subsurface conductivity. Such effects may introduce addi-
311 tional variability into the magnetometer signal that is not of external (ionospheric or magnetospheric) origin. However, since
312 the Entoto Magnetometer Station operates as a variometer (rather than a full absolute observatory), its primary role is to cap-
313 ture temporal variations in the geomagnetic field. The expected induction effects are therefore not anticipated to compromise
314 the station's scientific objectives, which focus on monitoring dynamic current systems like the Equatorial Electrojet (EEJ) and
315 storm-time magnetospheric responses.

316 Nevertheless, to improve the long-term reliability and data quality of the station, a future relocation ("lift and shift") is
317 planned. The Entoto Observatory is currently undergoing expansion on its western side, where new perimeter fencing is being
318 erected for improved security. The expanded area will allow for the installation of magnetometer infrastructure with a mini-
319 mum clearance of 100 m from nearby buildings, fences, or ferromagnetic structures — meeting the site criteria recommended
320 for modern observatories. This future upgrade will further reduce the influence of induction from local anomalies.

321 Despite these challenges, further analysis across several geomagnetic storms revealed prompt increases across all field
322 components, confirming the station's responsiveness to magnetospheric disturbances. The performance of the local K-index,
323 though influenced by EEJ effects, demonstrates Entoto's capability to provide meaningful space weather data, aligning with
324 methods applied in other equatorial observatories (Myint et al., 2022b). The combination of CHAOS 8.2 internal and external
325 field corrections, high-pass filtering, and preliminary regional K-index estimation forms a framework for interpreting magnetic
326 field variations at this station, and creates a foundation for future upgrades.

327 Initial results demonstrate the station's ability to detect and characterize geomagnetic disturbances, with observed field
328 changes aligning well with Dst index variations. The correlation between magnetospheric signals and global disturbance indices
329 suggests that the Entoto station is sensitive to space weather drivers, hence proves useful for regional monitoring.

330 As the only current equatorial station on the African continent, the Entoto Magnetometer Station plays a critical role in
331 addressing current gaps in longitudinal geomagnetic data. Its location on the magnetic equator enables detailed observations
332 of equatorial ionospheric phenomena, including the Equatorial Electrojet (EEJ) and Sq currents, which are poorly resolved by
333 mid- and high-latitude stations.

334 The computation of a local K-index using a historical L_9 threshold of 242 nT, based on the former AAE magnetic observatory
335 15 kilometres away from the newly deployed station, highlights both the value and limitations of such metrics in equatorial
336 regions. While the local K-index was consistently higher than the global Kp, this discrepancy, also observed in other studies
337 (Myint et al., 2022b), underscores the need to determine a site-specific L_9 value for Entoto. However, the day-to-day variability
338 introduced by the EEJ makes this a challenging task.

339 The comparison between the station's magnetospheric signal and the Dst index, along with the observed differences in EEJ
340 amplitude during quiet and disturbed periods, highlights the capability of the Entoto Magnetometer Station to capture both
341 global and regional geomagnetic variations.

342 So despite some challenges, the observed responses to geomagnetic storms, the correlation with Dst, and the strong perfor-
343 mance of the preliminary K-index estimation all confirm the Entoto station's potential to deliver accurate and valuable space
344 weather measurements. These results mark an important milestone for geomagnetic monitoring in Africa and demonstrate the
345 station's readiness to contribute to the global geomagnetic network.

346 **6 Future Work**

347 While the initial results have focused on geomagnetic field variations, future studies will expand to include a deeper analysis
348 of ionospheric effects, such as the Equatorial Electrojet (EEJ) and Sq variations. These phenomena are of particular interest for
349 understanding how space weather affects the African sector. It is also imperative to calculate a local L_9 value. Additionally,
350 there is potential for expanding the network of magnetometer stations across Africa to improve longitudinal data coverage.
351 The deployment of the Entoto Magnetometer Station marks a significant milestone in geomagnetic monitoring in the African
352 region, but we also acknowledge the valuable foundation laid by previous magnetometer deployment initiatives across the
353 African continent, including the AMBER network, whose efforts have informed our current approach. Drawing from these
354 lessons, the Entoto station is supported by a formal Memorandum of Understanding (MoU) between SANSA and SSGI, en-
355 suring long-term institutional engagement. Key to this partnership is ongoing, transparent communication across research and
356 technical teams, enabling shared responsibility in both instrument maintenance and data utilisation. This collaborative model
357 avoids silo-ed operations and fosters local capacity development. To support this, SANSA and SSGI continue to jointly apply
358 for travel and training grants to facilitate technical workshops and ensure long-term sustainability.

359 Our initial results show that the station is well-equipped to contribute valuable data to global space weather research. With
360 future expansions and collaborations, this station will play an increasingly important role in understanding geomagnetic and
361 ionospheric phenomena in this critical region.

362 **Author Contribution**

363 AN, NG, ZI, and DC were responsible for the deployment of the Entoto station. MS, OB, and JM contributed to the processing
364 of raw data into IAGA format and supported the development and operation of the data transfer software. AN performed the
365 data analysis and drafted the results and conclusions sections.

366 **Competing Interests**

367 The authors declare that there are no competing interests.

368 **Data Availability**

369 The data from the Entoto Magnetometer Station will be made available to the scientific community for non-commercial re-
370 search purposes upon reasonable request to the corresponding author.

371 *Acknowledgements.* The authors would like to acknowledge **Leonhardt Roman** for developing and maintaining the *MagPy* software suite,
372 which was instrumental in processing and analyzing magnetic field data for this study. We thank **Chane Moges** and **Yekoye Tariku** for
373 their assistance during the deployment of the magnetometer. We also extend our sincere thanks to **Emmanuel Nahayo** at the *South African*
374 *National Space Agency (SANSA)* for his support in assessing the preliminary geomagnetic measurements from the Entoto station. Also **Oliver**
375 **Bronkala** of the GFZ who assisted in transferring the data to a dedicated server.

376 We acknowledge the use of the *CHAOS* geomagnetic field model, developed and maintained by the *Technical University of Denmark*
377 (*DTU*), which was used to remove field contributions from the observations. We further acknowledge the providers of geomagnetic indices:
378 the **Dst index** supplied by the *World Data Center for Geomagnetism, Kyoto*, and the **Ap index** provided by the *GFZ German Research Centre*
379 *for Geosciences* in Potsdam.

380 The Entoto dual magnetometer station is operated with the support of the *Entoto Observatory and Research Center*, with technical
381 collaboration from *SANSA* and *GFZ Potsdam*. We also acknowledge the *INTERMAGNET* network and its data standards, which served as a
382 reference framework during quality assurance.

383 This research made extensive use of open-source tools, including *Python*, *pandas*, *matplotlib*, and *SciPy*, and we gratefully
384 acknowledge the open-science community for their contributions. The author(s) acknowledge the use of the AI language model ChatGPT for
385 assistance with Python syntax correction and Grammarly for language refinement in the preparation of this manuscript.

- 387 Constable, C. G. and Constable, S. C. (2023). A grand spectrum of the geomagnetic field. *Physics of the Earth and Planetary Interiors*,
388 344:107090.
- 389 Denardini, C. M., da Silva, M. R., Gende, M. A., Chen, S. S., Fagundes, P. R., Schuch, N. J., Petry, A., Resende, L. C. A., Moro, J., Padilha,
390 A. L., Sant'Anna, N., and Alves, L. R. (2015). The initial steps for developing the south american k index from the embrace magnetometer
391 network. *Revista Brasileira de Geofísica*, 33(1):79–88.
- 392 Finlay, C. C., Kloss, C., Olsen, N., Hammer, M. D., Tøffner-Clausen, L., Grayver, A. V., and Kuvshinov, A. (2020). The chaos-7 geomagnetic
393 field model and observed changes in the south atlantic anomaly. *Earth, Planets and Space*, 72(1):156.
- 394 Forbes, J. M. and Lindzen, R. S. (1981). Solar semidiurnal tide in the thermosphere. *Journal of Atmospheric and Terrestrial Physics*,
395 43(5-6):407–413.
- 396 Giday, N. M., Katamzi-Joseph, Z. T., and Stoneback, R. (2020). Effect of moderate geomagnetic storms on equatorial plasma bubbles over
397 eastern africa in the year 2012: Evolution and electrodynamics. *Advances in Space Research*, 65(7):1701–1713.
- 398 Habarulema, J. B., Lefebvre, G., Moldwin, M. B., Katamzi-Joseph, Z. T., and Yizengaw, E. (2019). Counter-electrojet occurrence as observed
399 from c/nofs satellite and ground-based magnetometer data over the african and american sectors. *Space Weather*, 17(7):1090–1104.
- 400 Hamid, N. S. A., Liu, H., Uozumi, T., Yumoto, K., Veenadhari, B., Yoshikawa, A., and Sanchez, J. A. (2014a). Relationship between the
401 equatorial electrojet and global sq currents at the dip equator region. *Earth, Planets and Space*, 66(1):146.
- 402 Hamid, N. S. A., Liu, H., Uozumi, T., Yumoto, K., Veenadhari, B., Yoshikawa, A., and Sanchez, J. A. (2014b). Relationship between the
403 equatorial electrojet and global sq currents at the dip equator region. *Earth, Planets and Space*, 66(1):146. Received: 31 March 2014;
404 Accepted: 16 October 2014; Published: 29 October 2014.
- 405 Jankowski, J. and Sucksdorf, C. (1996). *Guide for Magnetic Measurements and Observatory Practice*, volume 5 of *IAGA Guide*. International
406 Association of Geomagnetism and Aeronomy (IAGA), Warsaw, Poland. IAGA, Publication Office, Warszawa, 110 pp.
- 407 Kamide, Y. (2001). *Geomagnetic Storms as a Dominant Component of Space Weather: Classic Picture and Recent Issues*, pages 43–77.
408 Springer Netherlands, Dordrecht.
- 409 Kloss, C., Finlay, C. C., Olsen, N., Tøffner-Clausen, L., Gillet, N., and Grayver, A. (2025). Chaos-8.2 geomagnetic field model. *Earth*,
410 *Planets and Space*, 77:67.
- 411 Korte, M., Manda, M., Kotzé, P., and Menvielle, M. (2018). The geomagnetic observatory network and its evolution. *Annales Geophysicae*,
412 36:1327–1343.
- 413 Korte, M., Manda, M., Linthe, H.-J., Hemshorn, A., Kotzé, P., and Ricaldi, E. (2009). New geomagnetic field observations in the south
414 atlantic anomaly region. *Annals of Geophysics*, 52(1):65–81.
- 415 Kotzé, P. B., Cilliers, P. J., and Sutcliffe, P. R. (2015). The role of sansa's geomagnetic observation network in space weather monitoring: A
416 review. *Space Weather*, 13(10):656–664.
- 417 Macmillan, S. (2007). *Observatories: an overview*. Springer.
- 418 Matzka, J., Chulliat, A., Manda, M., Finlay, C. C., and Qamili, E. (2010). Geomagnetic observations for main field studies: From ground to
419 space. *Space Science Reviews*, 155(1-4):29–64.
- 420 Menvielle, M., Papitashvili, N., Häkkinen, L., and Sucksdorff, C. (1995). Computer production of k indices: review and comparison of
421 methods. *Geophysical Journal International*, 123(3):866–886.

422 Mungufeni, P., Habarulema, J. B., Migoya-Orué, Y., and Jurua, E. (2018). Statistical analysis of the correlation between the equatorial
423 electrojet and the occurrence of the equatorial ionisation anomaly over the east african sector. *Annales Geophysicae*, 36(3):841–853.

424 Myint, L. M., Hozumi, K., Saito, S., and Supnithi, P. (2022a). Analysis of local geomagnetic index under the influence of equatorial electrojet
425 (eej) at the equatorial phuket geomagnetic station in thailand. *Advances in Space Research*, 70(5):1429–1440.

426 Myint, L. M., Hozumi, K., Saito, S., and Supnithi, P. (2022b). Analysis of local geomagnetic index under the influence of equatorial electrojet
427 (eej) at the equatorial phuket geomagnetic station in thailand. *Advances in Space Research*, 70(5):1429–1440.

428 Nel, A. E. and Kotzé, P. B. (2024). A comparative investigation of geomagnetic jerks across the saa during the period 2000–2020. *Geophysical*
429 *Journal International*, 239(1):192–200.

430 Nel, A. E., Morschhauser, A., Vervelidou, F., and Matzka, J. (2024). A new high-resolution geomagnetic field model for southern africa.
431 *South African Journal of Science*, 120(1/2).

432 Onwumechili, C. A. (1997a). *The Equatorial Electrojet*. Gordon and Breach Science Publishers.

433 Onwumechili, C. A. (1997b). *The Equatorial Electrojet*. Gordon and Breach Science Publishers, Amsterdam.

434 Rangarajan, G. K., Iyemori, T., and Yumoto, K. (2002). Estimation of sq and eej currents and their seasonal variation using ground-based
435 magnetic data. *Earth, Planets and Space*, 54(5):527–538.

436 Stolle, C., Michaelis, I., and Reda, J. (2018). MagPy - Magnetometer Python Toolbox.

437 Sucksdorff, C., Pirjola, R., and Häkkinen, L. (1991). Computer production of k-indices based on linear elimination. *Geophysical Transac-*
438 *tions*, 36(3-4):335–345.

439 Sugiura, M. (1964). Hourly values of equatorial dst for the igy. *Annals of the International Geophysical Year*, 35:9–45.

440 Uemoto, J., Maruyama, T., Saito, S., Ishii, M., and Yoshimura, R. (2010). Relationships between pre-sunset electrojet strength, pre-reversal
441 enhancement and equatorial spread-f onset. *Annales Geophysicae*, 28(2):449–454.

442 Yamazaki, Y. and Maute, A. (2016). Sq and eej—a review on the daily variation of the geomagnetic field caused by ionospheric dynamo
443 currents. *Space Science Reviews*, 201(1-4):1–186.

444 Yizengaw, E. and Moldwin, M. B. (2009). African meridian b-field education and research (amber) array. *Earth, Moon, and Planets*,
445 104(1-4):237–246.